Carl Zeiss

Confocal Laser Scanning Microscopy

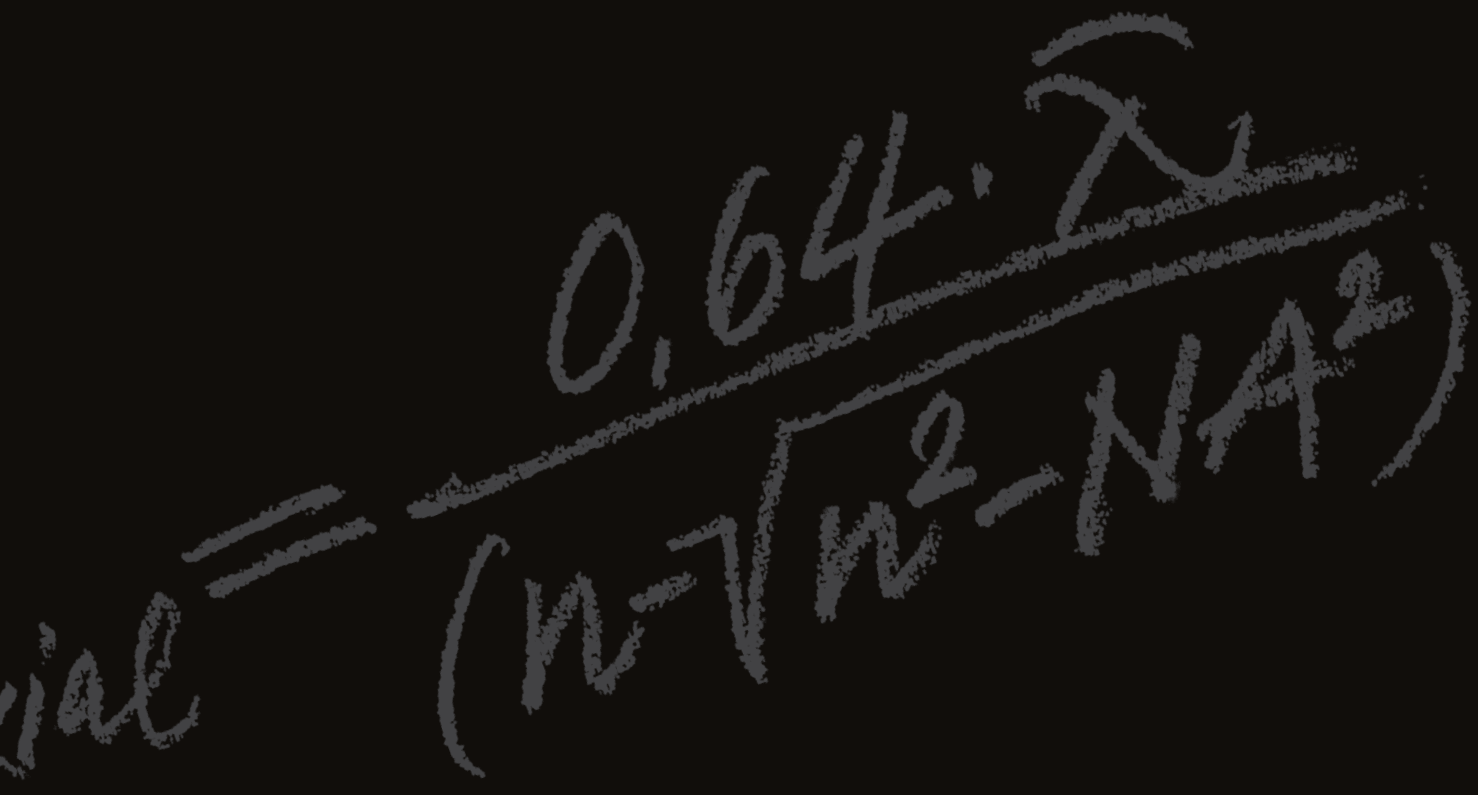

We make it visible.

Confocal Laser Scanning Microscopy

Stefan Wilhelm

Carl Zeiss Microscopy GmbH · Carl-Zeiss-Promenade 10 · 07745 Jena · Germany

In recent years, the confocal Laser Scanning Microscope (LSM) has become widely established as a research instrument.

The present brochure aims at giving a scientifically sound survey of the special nature of image formation in a confocal LSM.

Introduction

Following a description of the fundamental differences between a conventional and a confocal microscope, this monograph will set out the special features of the confocal LSM and the capabilities resulting from them.
The conditions in fluorescence applications will be given priority treatment throughout.

Image generation

The complete generation of the two-dimensional object information from the focal plane (object plane) of a confocal LSM essentially comprises three process steps:

1. Line-by-line scanning of the specimen with a focused laser beam deflected in the X and Y directions by means of two galvanometric scanners.
2. Detection of the fluorescence emitted by the scanned specimen details, by means of a photomultiplier tube (PMT).
3. Digitization of the object information contained in the electrical signal provided by the PMT (for presentation, the image data are displayed, pixel by pixel, from a digital matrix memory to a monitor screen).

Fig. 1 The quality of the image generated in a confocal LSM is not only influenced by the optics (as in a conventional microscope), but also, e.g., by the confocal aperture (pinhole) and by the digitization of the object information (pixel size). Another important factor is noise (laser noise, or the shot noise of the fluorescent light). To minimize noise, signal-processing as well as optoelectronic and electronic devices need to be optimized.

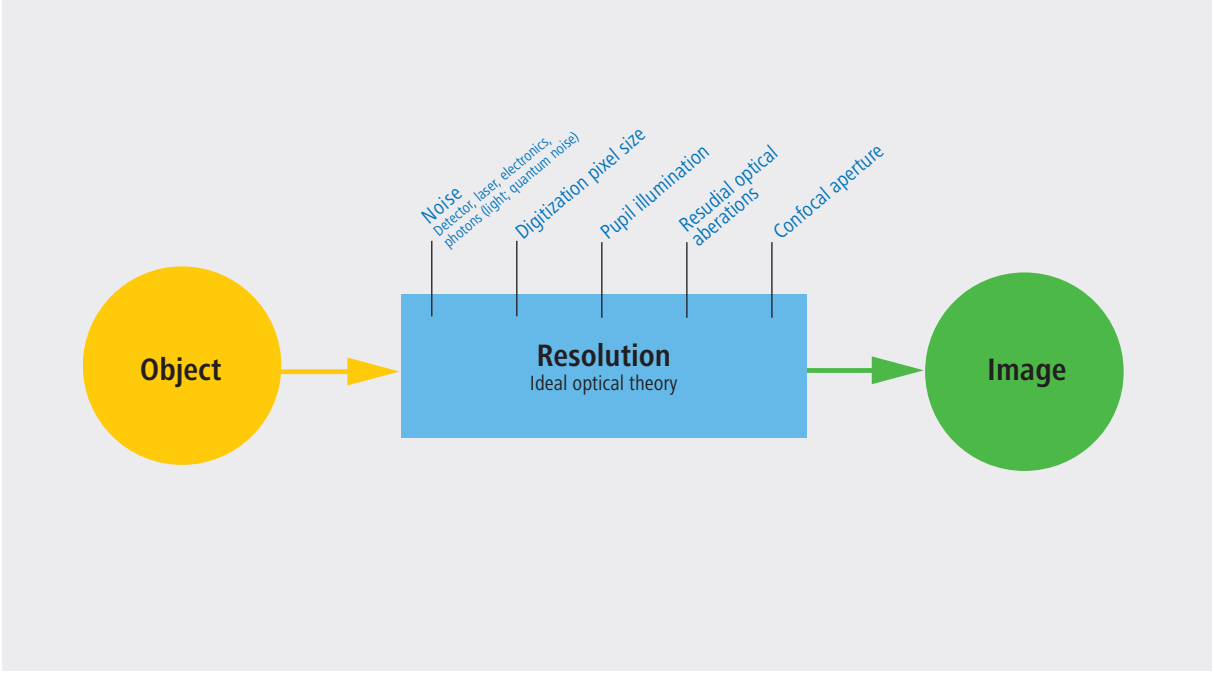

Scanning process

In a conventional light microscope, object-to-image transformation takes place simultaneously and parallel for all object points. By contrast, the specimen in a confocal LSM is irradiated in a pointwise fashion, i.e. serially, and the physical interaction between the laser light and the specimen detail irradiated (e.g. fluorescence) is measured point by point. To obtain information about the entire specimen, it is necessary to guide the laser beam across the specimen, or to move the specimen relative to the laser beam, a process known as scanning. Accordingly, confocal systems are also known as point-probing scanners.
To obtain images of microscopic resolution from a confocal LSM, a computer and dedicated software are indispensable. The descriptions below exclusively cover the point scanner principle as implemented, for example, in laser scanning microscopes from Carl Zeiss. Configurations in which several object points are irradiated simultaneously are not considered.

Confocal beam path

The decisive design feature of a confocal LSM compared with a conventional microscope is the confocal aperture (usually called pinhole) arranged in a plane conjugate to the intermediate image plane and, thus, to the object plane of the microscope. As a result, the detector (PMT) can only detect light that has passed the pinhole. The pinhole diameter is variable; ideally, it is infinitely small, and thus the detector looks at a point (point detection).
As the laser beam is focused to a diffraction-limited spot, which illuminates only a point of the object at a time, the point illuminated and the point observed (i.e. image and object points) are situated in conjugate planes, i.e. they are focused onto each other. The result is what is called a confocal beam path (see figure 2).

Pinhole

Depending on the diameter of the pinhole, light coming from object points outside the focal plane is more or less obstructed and thus excluded from detection. As the corresponding object areas are invisible in the image, the confocal microscope can be understood as an inherently depth-discriminating optical system.
By varying the pinhole diameter, the degree of confocality can be adapted to practical requirements. With the aperture fully open, the image is nonconfocal. As an added advantage, the pinhole suppresses stray light, which further improves image contrast.

Fig. 2 Beam path in a confocal LSM. A microscope objective lens is used to focus a laser beam onto the specimen, where it excites fluorescence, for example. The fluorescent radiation is collected by the objective and efficiently directed onto the detector via a dichroic beamsplitter. The interesting wavelength range of the fluorescence spectrum is selected by an emission filter, which also acts as a barrier, blocking the excitation laser line. The pinhole is arranged in front of the detector, on a plane conjugate to the focal plane of the objective lens. Light coming from planes above or below the focal plane is out of focus when it hits the pinhole, so most of it cannot pass the pinhole and therefore does not contribute to forming the image.

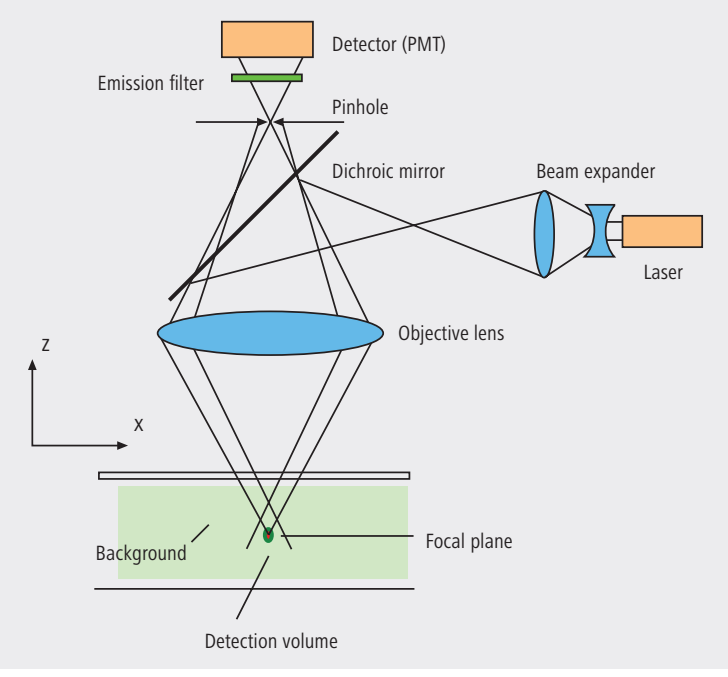

Optical slices

With a confocal LSM and it's variable pinhole it is therefore possible to exclusively image a thin optical slice out of a thick specimen (typically, up to 100 µm), a method known as optical sectioning. Under suitable conditions, the thickness (Z dimension) of such a slice may be less than 500 nm. The fundamental advantage of the confocal LSM over a conventional microscope is obvious: In conventional fluorescence microscopy, the image of a thick biological specimen will only be in focus if its Z dimension is not greater than the wave-optical depth of focus specified for the respective objective lens.
Unless this condition is satisfied, the in-focus image information from the object plane of interest is mixed with out-of focus image information from planes outside the focal plane. This reduces image contrast and increases the share of stray light detected. If multiple fluorescences are observed, there will in addition be a color mix of the image information obtained from the channels involved (figure 3, left).

Hence it follows that a confocal LSM can be used to advantage especially where thick fluorescent specimens (such as biological cells in tissue) have to be examined. The possibility of optical sectioning eliminates the drawbacks attached to the observation of such specimens by conventional fluorescence microscopy. With multicolor fluorescence, the various channels are furthermore satisfactorily separated and can be recorded simultaneously.
Figure 3 (right) demonstrates this capability of a confocal Laser Scanning Microscope.

Fig. 3 Non-confocal (left) and confocal (right) image of a triple-labeled cell aggregate (mouse intestine section). In the non-confocal image, specimen planes outside the focal plane degrade the information of interest from the focal plane, and differently stained specimen details appear in mixed color. In the confocal image (right), specimen details blurred in non-confocal imaging become distinctly visible, and the image throughout is greatly improved in contrast.

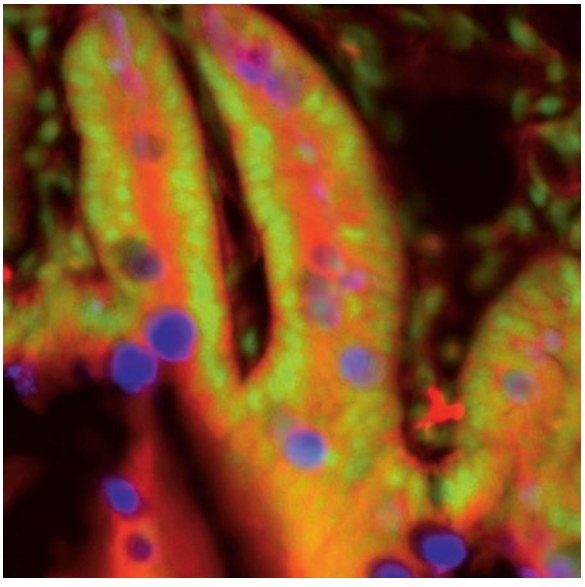

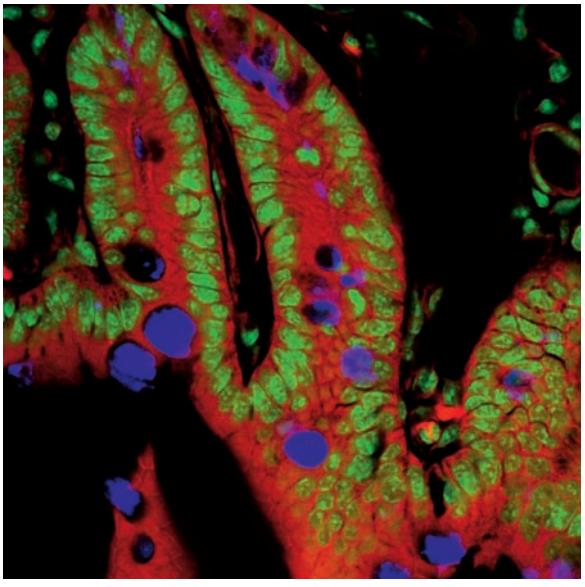

3rd dimension

In addition to the possibility to observe a single plane (or slice) of a thick specimen in good contrast, optical sectioning allows a great number of slices to be cut and recorded at different Z-planes of the specimen, with the specimen being moved along the optical axis by controlled increments. The result is a 3D data set, which provides information about the spatial structure of the object. The quality and accuracy of this information depend on the thickness of the slice and on the spacing between successive slices (optimum scanning rate in Z direction = 0.5x the slice thickness). By computation, various aspects of the object can be generated from the 3D data set (3D reconstruction, sections of any spatial orientation, stereo pairs etc.). Figure 4 shows a 3D reconstruction computed from a 3D data set.

Time series

A further field of importance is the investigation of living specimens that show dynamic changes even in the range of microseconds. Here, the acquisition of time-resolved confocal image series (known as time series) provides a possibility of visualizing and quantifying the changes (figure 5).

Spectral Imaging

The detection of spectral information becomes necessary when overlapping emission signals of multiple marked specimen are to be separated. By means of a special Multichannel PMT it is possible to record the spectral information of the fluorescent signal. Together with advanced computation methods one can separate signals which almost overlap completely and only differ in their spectral signature. The method behind is called ''linear unmixing'' and allows, for example, several fluorescent proteins to be distinguished.

Fig. 4 3D projection reconstructed from 108 optical slices of a three-dimensional data set of epithelium cells of a lacrimal gland. Actin filaments of myoepithelial cells marked with BODIPY-FL phallacidin (green), cytoplasm and nuclei of acinar cells with ethidium homodimer-1 (red).

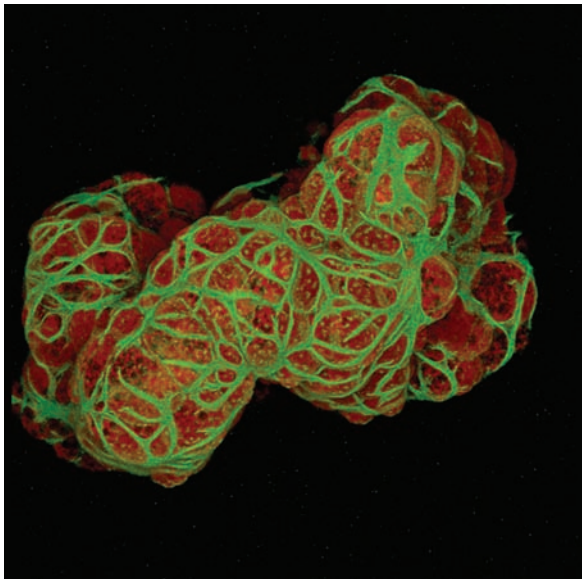

Fig. 5 Gallery of a time series experiment with Kaede-transfected cells. By repeated activation of the Kaede marker (green-to-red color change) in a small cell region, the entire green fluorescence is converted step by step into the red fluorescence.

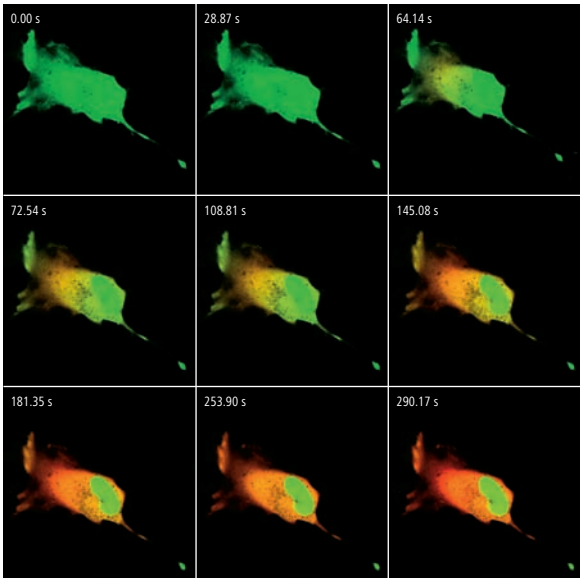

Point Spread Function

In order to understand the optical performance characteristics of a confocal LSM in detail, it is necessary to have a closer look at the fundamental optical phenomena resulting from the geometry of the confocal beam path. As mentioned before, what is most essential about a confocal LSM is that both illumination and observation (detection) are limited to a point.

Not even an optical system of diffraction-limited design can image a truly point-like object as a point. The image of an ideal point object will always be somewhat blurred, or "spread" corresponding to the imaging properties of the optical system. The image of a point can be described in quantitative terms by the point spread function (PSF), which maps the intensity distribution in the image space.

Where the three-dimensional imaging properties of a confocal LSM are concerned, it is necessary to consider the 3D-PSF.

In the ideal, diffraction-limited case (no optical aberrations, and homogeneous illumination at all lens cross sections – see Part 3 "Pupil Illumination"), the 3D-PSF is of comet-like, rotationally symmetrical shape.

For illustration, Figure 6 shows two-dimensional sections (XZ and XY) through an ideal 3D-PSF.

From the illustration it is evident that the central maximum of the 3D-PSF, in which 86.5% of the total energy available in the pupil of the objective lens are concentrated, can be described as an ellipsoid of rotation. For considerations of resolution and optical slice thickness it is useful to define the half-maximum area of the ellipsoid, i.e. the well-defined area in which the intensity of the 3D PSF in axial and lateral direction has dropped to half of the central maximum.

Any reference to the PSF in the following discussion exclusively refers to the half-maximum area.

As said before the confocal LSM system as a whole generates two point images: one by projecting a point light source into the object space, the other by projecting a point detail of the object into the image space.

The total PSF (PSF_{tot}) of a confocal microscope behind the pinhole is composed of the PSFs of the illuminating beam path (PSF_{ill}; point illumination) and the detection beam path (PSF_{det}; point detection). Mathematically, this relationship can be described as follows:

$$PSF_{tot}(x,y,z) = PSF_{ill}(x,y,z) \cdot PSF_{det}(x,y,z) \quad (1)$$

PSF_{ill} corresponds to the light distribution of the laser spot that scans the object. It's size is mainly a function of the laser wavelength and the numerical aperture of the microscope objective lens. It is also influenced by diffraction at the objective lens pupil (as a function of pupil illumination, see details) and the aberrations of all optical components integrated in the system. [Note: In general, these aberrations are low, having been minimized during system design]. Moreover, PSF_{ill} may get deformed if the laser focus enters thick and light-scattering specimens, especially if the refractive indices of immersion liquid and mounting medium are not matched and/or if the laser focus is at a great depth below the specimen surface (see Hell, S., et al., [7]).

PSF_{det} is also influenced by all these factors and, additionally, by the pinhole size. For reasons of beam path efficiency (see Part 2), the pinhole is never truly a point of infinitely small size and thus PSF_{det} is never smaller in dimension than PSF_{ill}. It is evident that the imaging properties of a confocal LSM are determined by the interaction between PSF_{ill} and PSF_{det}. As a consequence of the interaction process, it can be written: $PSF_{tot} \leq PSF_{ill}$.

With the pinhole diameter being variable, the effects obtained with small and big pinhole diameters must be expected to differ. In the following sections, various system states are treated in quantitative terms.

From the explanations made so far, it can also be derived that the optical slice is not a sharply delimited body. It does not start abruptly at a certain Z position, nor does it end abruptly at another. Because of the intensity distribution along the optical axis, there is a continuous transition from object information suppressed and such made visible.

Accordingly, the out-of-focus object information actually suppressed by the pinhole also depends on the correct setting of the image processing parameters (PMT high voltage, contrast setting). Signal overdrive or excessive offset should be avoided.

Fig. 6a Section through the 3D-PSF in Z direction as generated by a diffraction limited objective lens – left, and in XY-direction – right (computed; dimensionless representation); the central, elliptical maximum is distinctly visible.

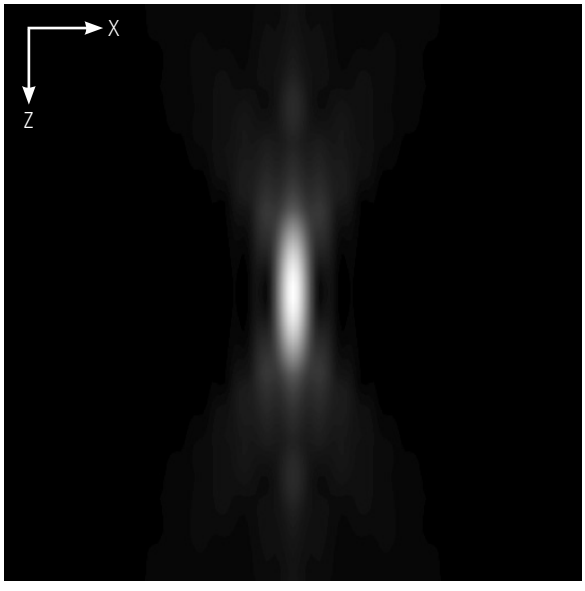

Fig. 6b The central maximum in this illustration is called Airy disk and is contained in the 3D-PSF as the greatest core diameter in lateral direction.

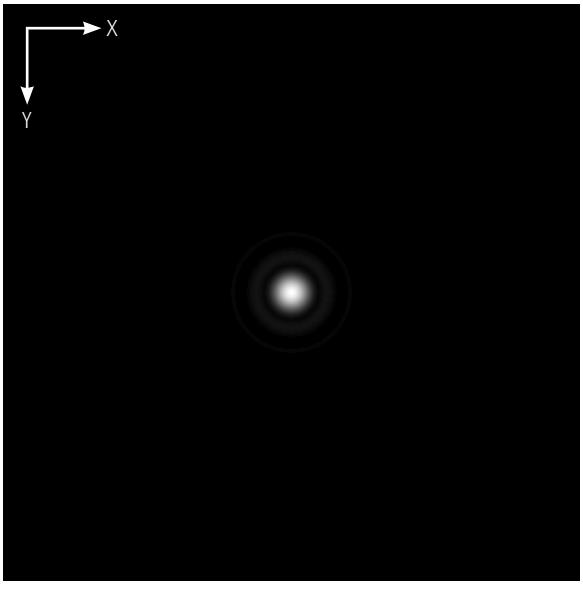

Resolution and Confocality

Wherever quantitative data on the resolving power and depth discrimination of a confocal LSM are specified, it is necessary to distinguish clearly whether the objects they refer to are point-like or extended, and whether they are reflective or fluorescent. These differences involve distinctly varying imaging properties. Fine structures in real biological specimens are mainly of a filiform or point-like fluorescent type, so that the explanations below are limited to point-like fluorescent objects. The statements made for this case are well applicable to practical assignments.

As already mentioned, the pinhole diameter plays a decisive role in resolution and depth discrimination. With a pinhole diameter greater than 1 AU (AU = Airy unit – *see Details "Optical Coordinates"*), the depth discriminating properties under consideration are essentially based on the law of geometric optics (geometric-optical confocality).

The smaller the pinhole diameter, the more PSF_{det} approaches the order of magnitude of PSF_{ill}. In the limit case (PH < 0.25 AU), both PSFs are approximately equal in size, and wave-optical image formation laws clearly dominate (wave-optical confocality).

Figure 7 illustrates these concepts. It is a schematic representation of the half-intensity areas of PSF_{ill} and PSF_{det} at selected pinhole diameters.

Depending on the pinhole diameter, the data and computation methods for resolution and depth discrimination will differ. A comparison with image formation in conventional microscopes is interesting as well. The following sections deal with this in detail.

Fig. 7 Geometric-optical (a) and wave-optical confocality (c) [XZ view].
The pinhole diameter decreases from (a) to (c).
Accordingly, PSF_{det} (green) shrinks until it approaches the order of magnitude of PSF_{ill} (red).

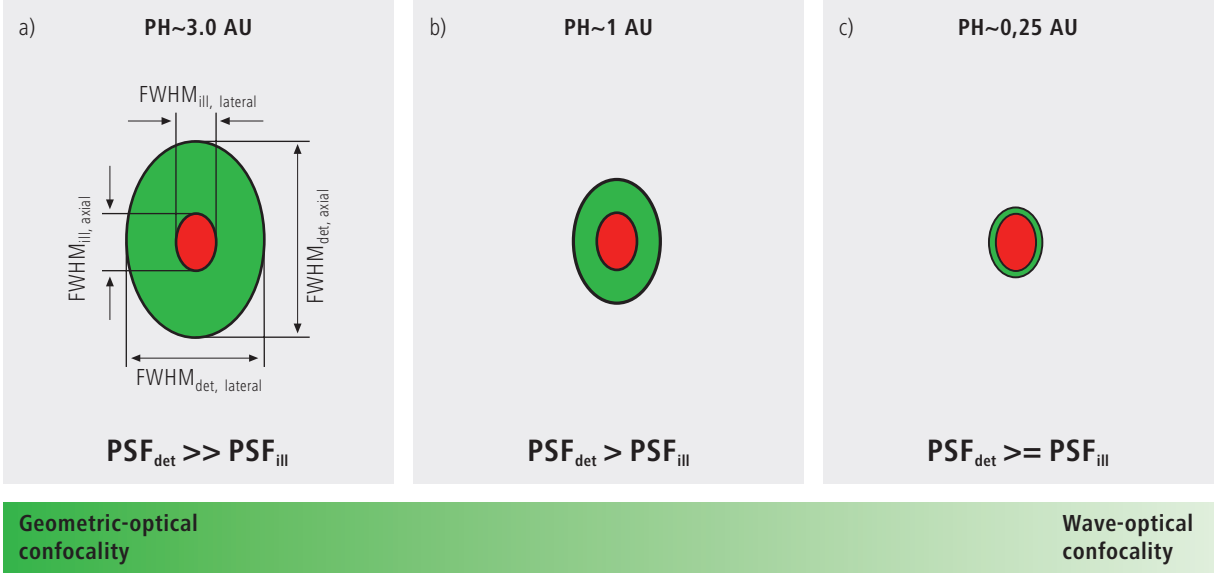

Resolution

Resolution, in case of large pinhole diameters (PH >1AU), is meant to express the separate visibility, both laterally and axially, of points during the scanning process. Imagine an object consisting of individual points: all points spaced closer than the extension of PSF_{ill} are blurred (spread), i.e. they are not resolved.

Quantitatively, resolution results from the axial and lateral extension of the scanning laser spot, or the elliptical half-intensity area of PSF_{ill}. On the assumption of homogeneous pupil illumination, the following equations apply:

Axial:

$$FWHM_{ill,axial} = \frac{0.88 \cdot \lambda_{exc}}{(n-\sqrt{n^2-NA^2})} \qquad (2)$$

n = *refractive index of immersion liquid*
NA = *numerical aperture of the objective*
λ_{exc} = *wavelength of the excitation light*

If NA < 0.5, equation (2) can be approximated by:

$$\approx \frac{1.77 \cdot n \cdot \lambda_{exc}}{NA^2} \qquad (2a)$$

Lateral:

$$FWHM_{ill,lateral} = 0.51 \ \frac{\lambda_{exc}}{NA} \qquad (3)$$

At first glance, equations (2a) and (3) are not different from those known for conventional imaging (see Beyer, H., [1]). It is striking, however, that the resolving power in the confocal microscope depends only on the wavelength of the illuminating light, rather than exclusively on the emission wavelength as in the conventional case.
Compared to the conventional fluorescence microscope, confocal fluorescence with large pinhole diameters leads to a gain in resolution by the factor ($\lambda_{em}/\lambda_{exc}$) via the stokes shift.

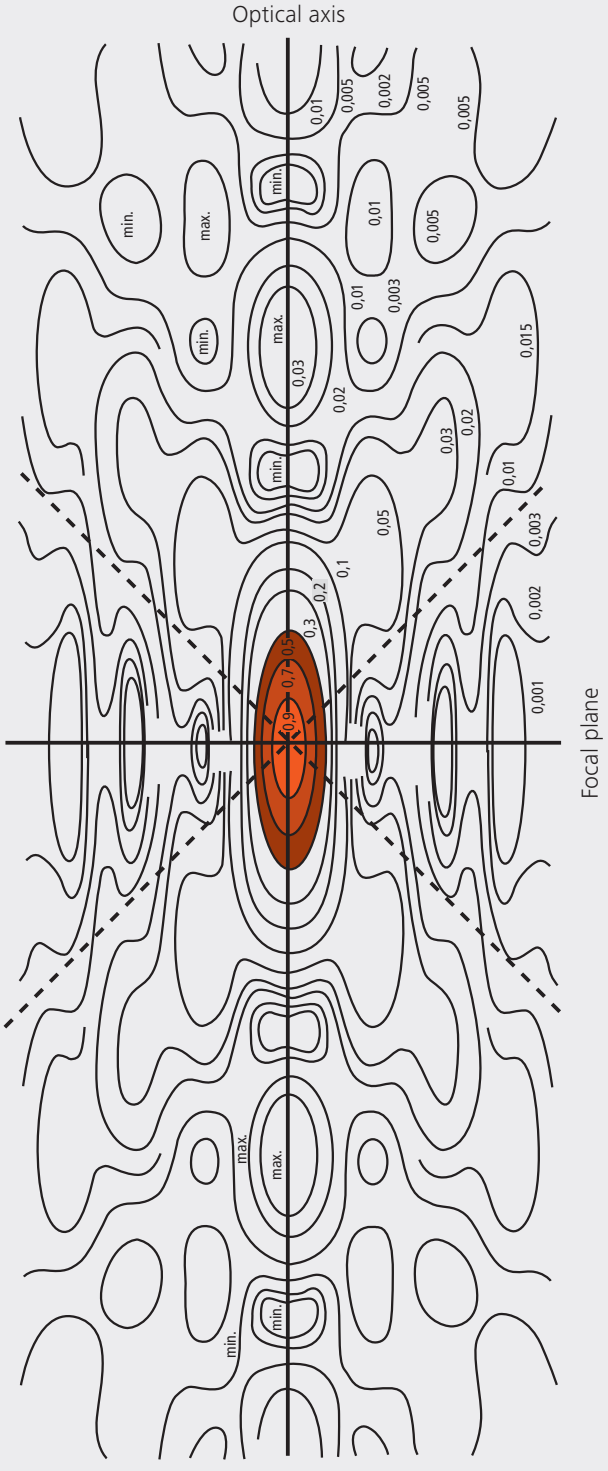

Let the statements made on the PSF so far be further illustrated by the figure on the left. It shows a section through the resulting diffraction pattern surrounding the focus on the illumination side (PSF_{ill}).

The lines include areas of equal brightness (isophote presentation). The center has a normalized intensity of 1. The real relationships result by rotation of the section about the vertical (Z) axis. Symmetry exists relative to the focal plane as well as to the optical axis. Local intensity maxima and minima are conspicuous. The dashed lines mark the range covered by the aperture angle of the microscope objective used.

For the considerations in this chapter, only the area marked in red color, i.e. the area at half maximum, is of interest.

Fig. 8 Isophote diagram of the intensity distribution around the illumination-side focus (PSF_{ill}). The intensity at the focus is normalized as 1. (Born & Wolf, Priniples of Optics, 6th edition 1988, Pergamon Press)

Geometric optical confocality

Optical slice thickness (depth discrimination) and stray light suppression (contrast improvement) are basic properties of a confocal LSM, even if the pinhole diameter is not an ideal point (i.e. not infinitely small). In this case, both depth discrimination and stray light suppression are determined exclusively by PSF_{det}. This alone brings an improvement in the separate visibility of object details over the conventional microscope.

Hence, the diameter of the corresponding half-intensity area and thus the optical slice thickness is given by:

$$FWHM_{det,axial} = \sqrt{\left(\frac{0.88 \cdot \lambda_{em}}{n-\sqrt{n^2-NA^2}}\right)^2 + \left(\frac{\sqrt{2} \cdot n \cdot PH}{NA}\right)^2} \quad (4)$$

λ_{em} = *emission wavelength*
PH = *object-side pinhole diameter [µm]*
n = *refractive index of immersion liquid*
NA = *numerical aperture of the objective*

Equation (4) shows that the optical slice thickness comprises a geometric-optical and a wave-optical term. The wave-optical term (first term under the root) is of constant value for a given objective and a given emission wavelength. The geometric-optical term (second term under the root) is dominant; for a given objective lens it is influenced exclusively by the pinhole diameter.

Likewise, in the case of geometric-optical confocality, there is a linear relationship between depth discrimination and pinhole diameter. As the pinhole diameter is constricted, depth discrimination improves (i.e. the optical slice thickness decreases). A graphical representation of equation (4) is illustrated in figure 9. The graph shows the geometric-optical term alone (blue line) and the curve resulting from eq. 4 (red line). The difference between the two curves is a consequence of the waveoptical term.
Above a pinhole diameter of 1 AU, the influence of diffraction effects is nearly constant and equation (4) is a good approximation to describe the depth discrimination. The interaction between PSF_{ill} and PSF_{det} becomes manifest only with pinhole diameters smaller than 1 AU.
Let it be emphasized that in case of geometric optical confocality the diameters of the half-intensity area of PSF_{det} allow no statement about the separate visibility of object details in axial and lateral direction.
In the region of the optical section ($FWHM_{det,axial}$), object details are resolved (imaged separately) only unless they are spaced not closer than described by equations (2) / (2a) / (3).

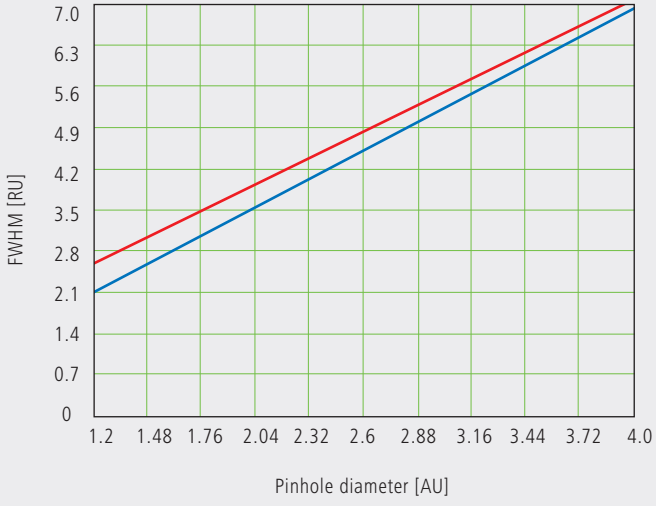

Fig.9 Optical slice thickness as a function of the pinhole diameter (red line). Parameters: NA = 0.6; n = 1; λ = 520 nm. The X axis is dimensioned in Airy units, the Y axis (slice thickness) in Rayleigh units (see also: Details "Optical Coordinates"). In addition, the geometric-optical term in equation 4 is shown separately (blue line).

Wave-optical confocality

If the pinhole is closed down to a diameter of <0.25 AU (virtually "infinitely small"), the character of the image changes. Additional diffraction effects at the pinhole have to be taken into account, and PSFdet (optical slice thickness) shrinks to the order of magnitude of PSF_{ill} (Z resolution) (see also figure 7c).

In order to achieve simple formulae for the range of smallest pinhole diameters, it is practical to regard the limit of PH = 0 at first, even though it is of no practical use. In this case, PSF_{det} and PSF_{ill} are identical. The total PSF can be written as:

$$PSF_{tot}(x,y,z) = \left(PSF_{ill}(x,y,z)\right)^2 \qquad (5)$$

In fluorescence applications it is furthermore necessary to consider both the excitation wavelength λ_{exc} and the emission wavelength λ_{em}. This is done by specifying a mean wavelength[1]:

$$\bar{\lambda} \approx \sqrt{2}\,\frac{\lambda_{em}\cdot\lambda_{exc}}{\sqrt{\lambda^2_{exc}+\lambda^2_{em}}} \qquad (6)$$

Thus, equations (2) and (3) for the widths of the axial and lateral half-intensity areas are transformed into:

Axial:

$$FWHM_{tot,axial} = \frac{0.64\cdot\bar{\lambda}}{(n-\sqrt{n^2-NA^2})} \qquad (7)$$

If NA < 0.5, equation (2) can be approximated by:

$$\approx \frac{1.28\cdot n\cdot\bar{\lambda}}{NA^2} \qquad (7a)$$

Lateral:

$$FWHM_{tot,lateral} = 0.37\,\frac{\bar{\lambda}}{NA} \qquad (8)$$

Note:
With the object being a mirror, the factor in equation 7 is 0.45 (instead of 0.64), and 0.88 (instead of 1.28) in equation 7a. For a fluorescent plane of finite thickness, a factor of 0.7 can be used in equation 7. This underlines that apart from the parameters (NA, $\bar{\lambda}$, n) influencing the optical slice thickness, the type of specimen also affects the measurement result.

[1] For rough estimates, the expression $\bar{\lambda} \approx \sqrt{\lambda_{em}\cdot\lambda_{exc}}$ suffices.

From equations (7) and (7a) it is evident that depth resolution varies linearly with the refractive index n of the immersion liquid and with the square of the inverse value of the numerical aperture of the objective lens {NA = n · sin(α)}.
To achieve high depth discrimination, it is important, above all, to use objective lenses with the highest possible numerical aperture.
As an NA > 1 can only be obtained with an immersion liquid, confocal fluorescence microscopy is usually performed with immersion objectives (see also figure 11).
A comparison of the results stated before shows that axial and lateral resolution in the limit case of PH=0 can be improved by a factor of 1.4. Furthermore it should be noted that, because of the wave-optical relationships discussed, the optical performance of a confocal LSM cannot be enhanced infinitely. Equations (7) and (8) supply the minimum possible slice thickness and the best possible resolution, respectively.

Fig. 10 Theoretical factors for equations (7) and (8), with pinhole diameters between 0 and 1 AU.

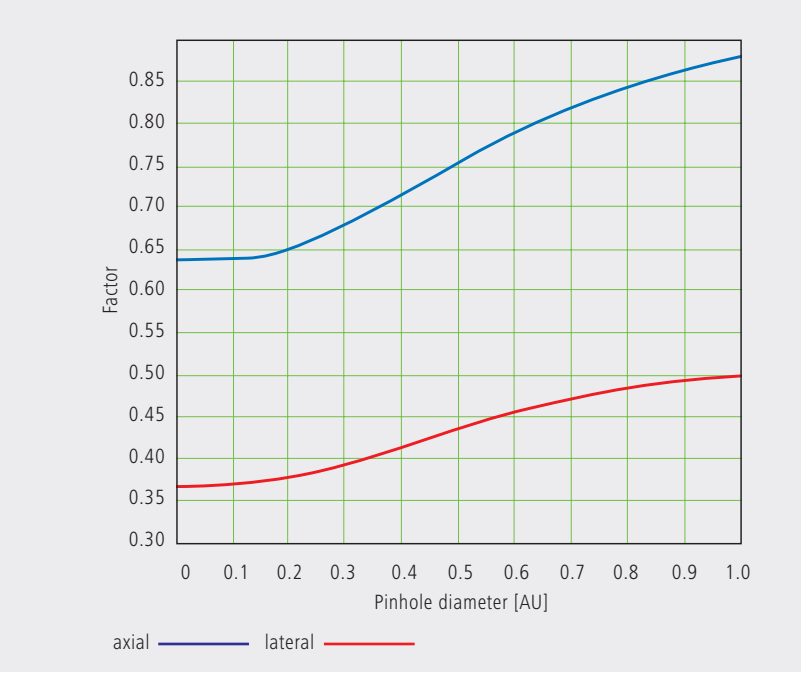

From the applications point of view, the case of strictly wave-optical confocality (PH=0) is irrelevant (see also Part 2). By merely changing the factors in equations (7) and (8) it is possible, though, to transfer the equations derived for PH=0 to the pinhole diameter range up to 1 AU, to a good approximation. The factors applicable to particular pinhole diameters can be taken from figure 10.

It must also be noted that with PH <1AU, a distinction between optical slice thickness and resolution can no longer be made. The thickness of the optical slice at the same time specifies the resolution properties of the system. That is why in the literature the term of depth resolution is frequently used as a synonym for depth discrimination or optical slice thickness. However, this is only correct for pinhole diameters smaller than 1 AU.

To conclude the observations about resolution and depth discrimination (or depth resolution), the table on page 17 provides an overview of the formulary relationships developed in Part 1. In addition, figure 11a (page 16) shows the overall curve of optical slice thickness for a microscope objective of NA = 1.3 and n = 1.52 ($\bar{\lambda}$ = 496 nm).
In figure 11 (b – d), equation (7) is plotted for different objects and varied parameters (NA, $\bar{\lambda}$, n).

Optical slice
(NA = 1.3; n = 1.52;
$\bar{\lambda}$ = 496 nm)

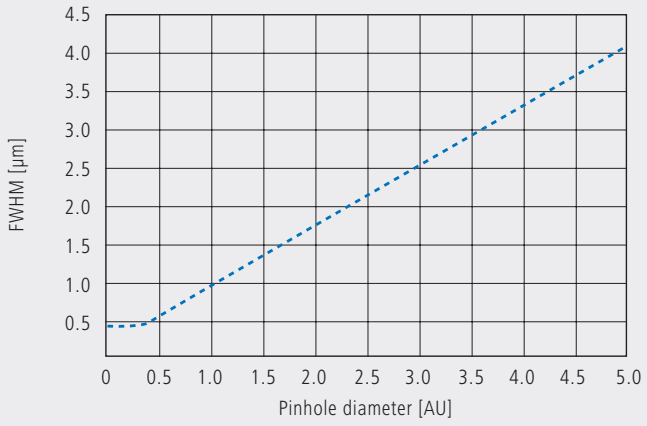

Fig. 11
a) Variation of pinhole diameter

Depth resolution
(PH = 0; n = 1.52;
$\bar{\lambda}$ = 496 nm)

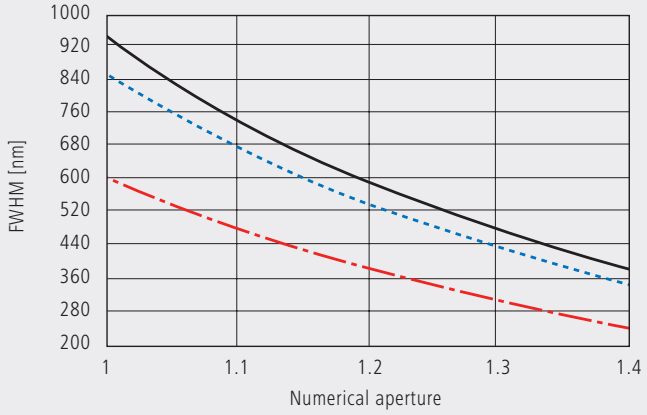

b) Variation of numerical aperture

Depth resolution
(PH = 0; NA = 1.3; n = 1.52)

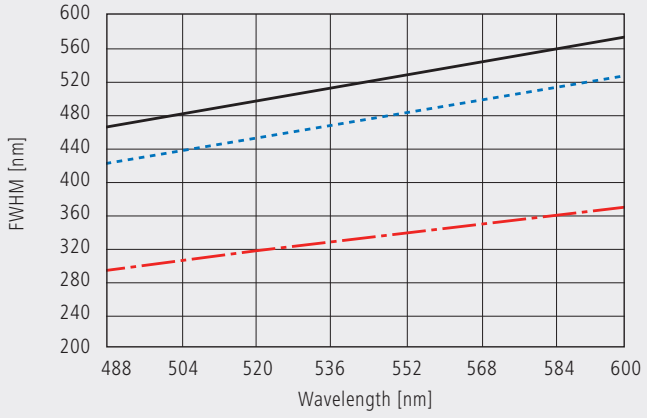

c) Variation of wavelength ($\bar{\lambda}$)

Depth resolution
(PH = 0; NA = 0.8;
$\bar{\lambda}$ = 496 nm)

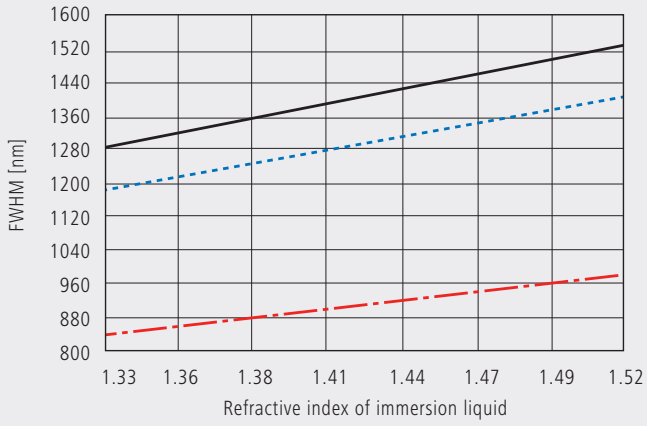

d) Variation of refractive index

fluorescent plane
fluorescent point
reflecting plane (mirror)

Overview

Conventional microscopy	Confocal microscopy 1 AU < PH <∞	Confocal microscopy PH < 0.25 AU
1. Optical slice thickness **not definable** With a conventional microscope, unlike in confocal microscopy, sharply defined images of "thick" biological specimens can only be obtained if their Z dimension is not greater than the wave-optical depth of field specified for the objective used. Depending on specimen thickness, object information from the focal plane is mixed with blurred information from out-of-focus object zones. Optical sectioning is not possible; consequently, no formula for optical slice thickness can be given.	1. Optical slice thickness1) $\sqrt{\left(\frac{0.88 \cdot \lambda_{em}}{(n-\sqrt{n^2-NA^2})}\right)^2+\left(\frac{\sqrt{2} \cdot n \cdot PH}{NA}\right)^2}$ Corresponds to the FWHM of the intensity distribution behind the pinhole (PSF_{det}). The FWHM results from the emission-side diffraction pattern and the geometric-optical effect of the pinhole. Here, PH is the variable object-side pinhole diameter in µm.	1. Optical slice thickness $\frac{0.64 \cdot \bar{\lambda}}{(n-\sqrt{n^2-NA^2})}$ The term results as the FWHM of the total PSF – the pinhole acts according to wave optics. $\bar{\lambda}$ stands for a mean wavelength – see text for the exact definition. The factor 0.64 applies only to a fluorescent point object.
2. Axial resolution (wave-optical depth of field) $\frac{n \cdot \lambda_{em}}{NA^2}$ Corresponds to the width of the emission-side diffraction pattern at 80% of the maximum intensity, referred to the object plane. In the literature, the wave-optical depth of field in a conventional microscope is sometimes termed depth resolution. However, a clear distinction should be made between the terms resolution and depth of field.	2. Axial resolution $\frac{0.88 \cdot \lambda_{exc}}{(n-\sqrt{n^2-NA^2})}$ FWHM of PSF_{ill} (intensity distribution at the focus of the microscope objective) in Z direction. No influence by the pinhole.	2. Axial resolution $\frac{0.64 \cdot \bar{\lambda}}{(n-\sqrt{n^2-NA^2})}$ FWHM of total PSF in Z direction As optical slice thickness and resolution are identical in this case, depth resolution is often used as a synonym.
3. For comparison: FWHM of PSF in the intermediate image (Z direction) – referred to the object plane. $\frac{1.77 \cdot n \cdot \lambda_{em}}{NA^2}$	3. Approximation to 2. for NA < 0.5 $\frac{1.77 \cdot n \cdot \lambda_{exc}}{NA^2}$	3. Approximation to 2. for NA < 0.5 $\frac{1.28 \cdot n \cdot \bar{\lambda}}{NA^2}$
4. Lateral resolution $\frac{0.51 \cdot \lambda_{em}}{NA}$ FWHM of the diffraction pattern in the intermediate image – referred to the object plane) in X/Y direction.	4. Lateral resolution $\frac{0.51 \cdot \lambda_{exc}}{NA}$ FWHM of PSF_{ill} (intensity distribution at the focus of the microscope objective) in X/Y direction plus contrast-enhancing effect of the pinhole because of stray light suppression.	4. Lateral resolution $\frac{0,37 \cdot \bar{\lambda}}{NA}$ FWHM of total PSF in X/Y direction plus contrast-enhancing effect of the pinhole because of stray light suppression.

All data in the table refer to quantities in the object space and apply to a fluorescent point object.
1) PH <∞ is meant to express a pinhole diameter of ≈ 4–5 AU.

Sampling and Digitization

After the optical phenomena have been discussed in Part 1, Part 2 takes a closer look at how the digitizing process and system-inherent sources of noise limit the performance of the system .

As stated in Part 1, a confocal LSM scans the specimen surface point by point. This means that an image of the total specimen is not formed simultaneously, with all points imaged in parallel (as, for example, in a CCD camera), but consecutively as a series of point images. The resolution obtainable depends on the number of points probed in a feature to be resolved.

Confocal microscopy, especially in the fluorescence mode, is affected by noise of light. In many applications, the number of light quanta (photons) contributing to image formation is extremely small. This is due to the efficiency of the system as a whole and the influencing factors involved, such as quantum yield, bleaching and saturation of fluorochromes, the transmittance of optical elements etc. (see Details "Fluorescence"). An additional factor of influence is the energy loss connected with the reduction of the pinhole diameter. In the following passages, the influences of scanning and noise on resolution are illustrated by practical examples and with the help of a two-point object. This is meant to be an object consisting of two self-luminous points spaced at 0.5 AU (see Details "Optical Coordinates"). The diffraction patterns generated of the two points are superimposed in the image space, with the maximum of one pattern coinciding with the first minimum of the other. The separate visibility of the points (resolution) depends on the existence of a dip between the two maxima (see figure 13, page 20).

The object information gained by the scanning process is, in most cases, detected by a photomultiplier tube (PMT), which registers the spatial changes of object properties I(x) as a temporal intensity fluctuation I(t). Spatial and temporal coordinates are related to each other by the speed of the scanning process ($x=t \cdot v_{scan}$). The cathode of the PMT converts optical information (photon) into electrical information (photoelectron), which is intensified in the following dynode cascade. The resulting continuous electric signal is periodically sampled by a subsequent analog-to-digital (A/D) converter and thus transformed into a discrete, equidistant succession of measured data (pixels) (figure 12).

Fig. 12 Pointwise sampling of a continuous signal
T = spacing of two consecutive sampling points
t = time of signal detection (t<<T)

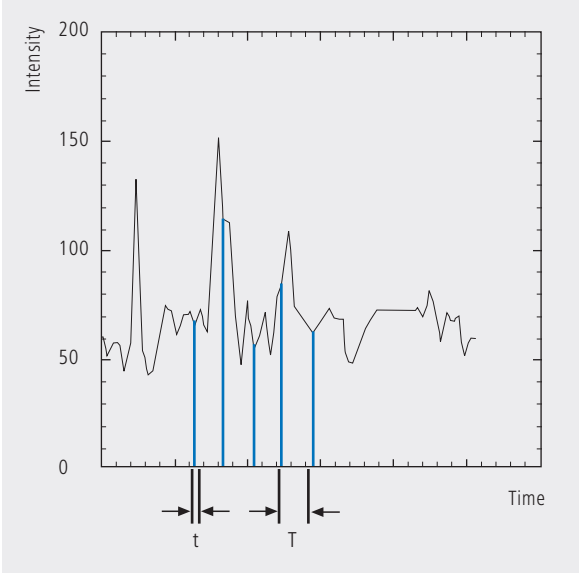

Types of A/D conversion

The quality of the image scanned depends on the type of A/D conversion which is employed. Two types can be distinguished:

- Sampling: The time (t) for signal detection (measurement) is small compared to the time (T) per cycle (pixel time) (see figure 12).
- Integration: The signal detection time has the same order of magnitude as the pixel time.

Integration is equivalent to an averaging of intensities over a certain percentage of the pixel time known as pixel dwell time. To avoid signal distortion (and thus to prevent a loss of resolution), the integration time must be shorter than the pixel time. The highest resolution is attained with point sampling (the sampling time is infinitesimally short, so that a maximum density of sampling points can be obtained). By signal integration, a greater share of the light emitted by the specimen contributes to the image signal. Where signals are weak (e.g. fluorescence), this is a decisive advantage over point sampling with regard to the signal-to-noise ratio (SNR). Therefore, Carl Zeiss confocal LSM systems operate in the integration mode. The absolute integration time can be modified by varying the scanning speed, which also means a change of the pixel time.

Nyquist theorem

It is known from Part 1 that the information content of the signal is limited by the resolving power of the microscope optics. A realistic estimate for the resolving power is the full width at half maximum intensity ($FWHM_{lat}$) of a point image (see equation 3).

To avoid a loss of information during the scanning process, it is necessary to stick to the Nyquist theorem. The optimal pixel spacing in scanning a periodic signal, as defined by the Nyquist theorem, is half the period of the feature spacing to be resolved, or two pixels per resolvable structure detail. Together with the resolving power defined above, this results in a maximum pixel spacing of $d_{pix} = 0.5 \times FWHM_{lat}$. With a two-point object (see explanation on page 18), the pixel spacing needed to separate the two Airy discs in the digitized image is 0.25 AU (figure 13).

If the number of sampling points per feature size is smaller than that given by the Nyquist theorem (undersampling), part of the information will be lost. This is evident in Figure 14c especially by the unresolved fine features.

A greater number of sampling points per feature size (oversampling) means a greater number of readings without a gain in information; simultaneously, the time per pixel becomes shorter. Thus, the volume of data to be processed is inflated, and the noise of the measurement signal increases (see page 22).

Under unfavorable conditions, also artefacts may result out of the digitization process (aliasing). As a rule, this is the case if the feature spacing in the specimen is equal, or nearly equal, to the pixel spacing.

Fig. 13 The graph illustrates the scanning of a two-point object with the minimum number of sampling points needed to avoid a loss of resolution (spacing of sampling points 0.25 AU).

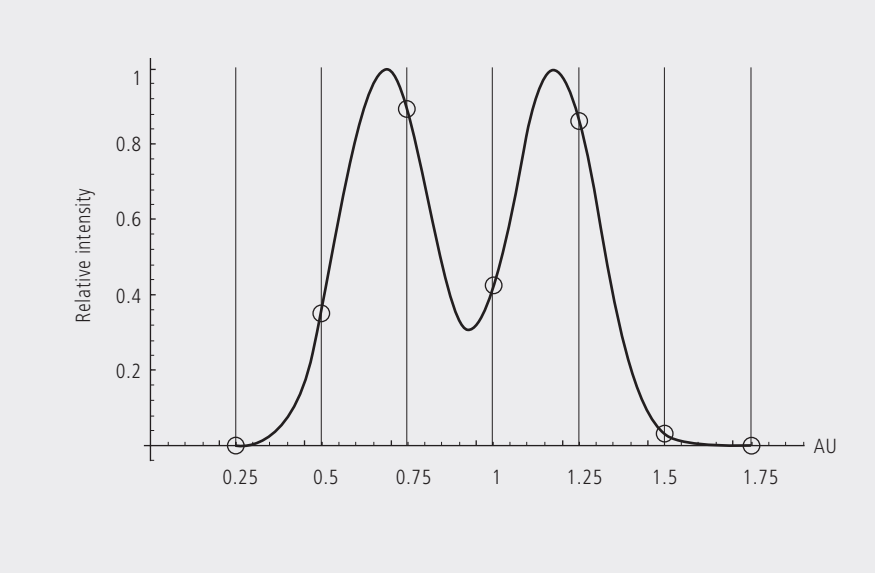

Fig. 14 Oversampling, correct sampling and undersampling of a continous signal.

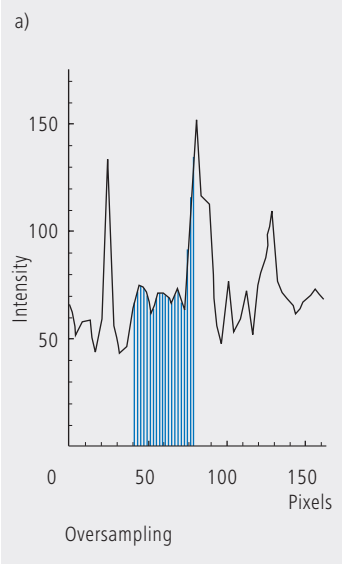

Pixel size

A quantity of decisive importance in this connection is the maximum scanning angle set via the scanning zoom. By varying the scanning angle, it is possible to directly influence the edge length of the scanned field in the intermediate image plane (or object plane), and thus the pixel size (at a given number of pixels per line). The smaller the scanning angle, the smaller is the edge length of the scanned field, and the smaller is the pixel (see the example below).
In this way, the user of a ZEISS confocal LSM can control the sampling rate (pixel size). For setting the suitable scanning zoom for correct Nyquist sampling, the pixel size d_{Pix} in the object plane is important.

For a ZEISS confocal LSM, there is a simple formula, based on the edge length of the scanned field in the intermediate image:

$$d_{pix} = \frac{\text{system constant}}{\text{number of pixels} \cdot \text{zoomfactor} \cdot \text{magnification}_{obj}}$$

Number of pixels *number of pixels per line*
Zoom factor (Z) *scanning zoom set in the software (Example: Zoom factor 2 reduces the edge length of the scanned field by a factor of 2)*
Magnification$_{obj}$ *objective magnification*

System constant

LSM 510, LSM 5 PASCAL	*8.94 mm*
LSM 700	*6.36 mm*
LSM 710 with Axio Observer	*10.08 mm (rearport)* *9.31 mm (sideport)*
LSM 710 with Axio Imager	*10.08 mm (rearport)* *9.31 mm (tube)*
LSM 710 with Axio Examiner	*6.85 mm*

The minimum scanning zoom needed to fullfill the Nyquist theorem can therefore be calculated as follows:

$$Z \geq \frac{3.92 \cdot NA \cdot \text{system constant}}{\text{number of pixels} \cdot \text{magnification}_{obj} \cdot \lambda_{exc}}$$

NA = numerical aperture of objective
λ_{exc} = excitation wavelength

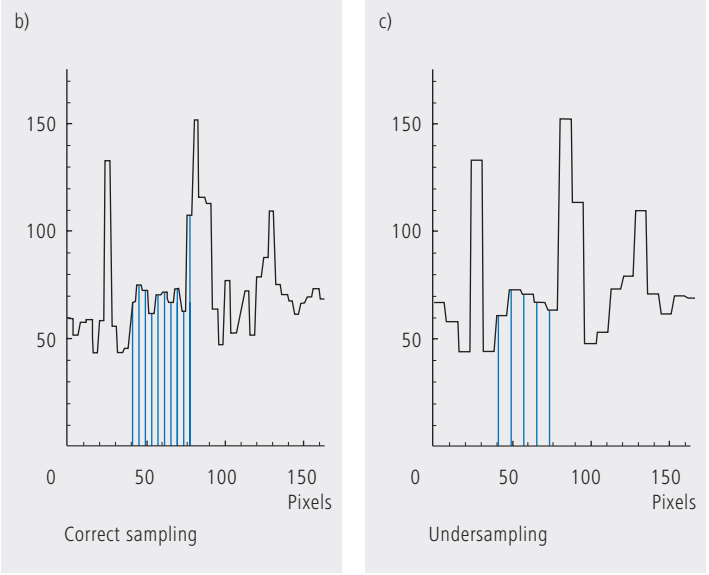

As an example, with the LSM 710 / Axio Observer (sideport), a 40x objective lens (NA=1.2), a wavelength of 488nm and 512 pixels per scanline, the full resolving power (correct sampling) is achieved with a scanning zoom of 4.38; the corresponding pixelsize then is 103.8nm. With lower factors of the scanning zoom the pixel size itself will be the limiting factor for resolution (pixel resolution). Higher factors will cause oversampling. Hence, the zoom factor influences not only the total magnification but also the resolution properties of the system.
With the more recent LSM systems from Carl Zeiss, the number of sampling points can also be influenced by an increase in the number of pixels per scan line.
(With the LSM 710 and LSM 780 the number of pixels (X/Y) per image can be freely selected between 4 x 1 and 6144 x 6144).

Noise

The main types of noise important in a confocal LSM system are detector noise (dark noise, secondary emission noise), laser noise, and shot noise of the light (see Details "Sources of Noise"). As a rule, these sources of noise are of a statistical nature. Periodic noise rarely occurs, and if it does, it tends to correlate with defective devices or mechanical vibration in the setup; therefore it has been left out of consideration here.

As said before the number of photons hitting the PMT depends not only on the intensity of the fluorescence signal (see Details "Fluorescence"), but also on the diameter of the pinhole. The graph in figure 15 show the intensity distribution of a two-point object resulting behind the pinhole, in normalized (left) and non-normalized form (right). The pinhole diameter was varied between 2 AU and 0.05 AU. At a diameter of 1 AU the pinhole just equals the size of the Airy disk, so that there is only a slight loss in intensity. The gain in lateral resolution, is minimum in this case.

With a pinhole diameter <1AU, resolution improves (better point separation thanks to a deeper dip), which is penalized by a drastic loss in energy.
Moreover, it should be considered that it depends on the signal level wich noise source dominates. With high-amplitude signals (number of detected photons >10.000), laser noise is the dominating effect, whereas the quality of low signals (number of detected photons <1000) is limited by the shot noise of the light.
Therefore, laser noise tends to be the decisive noise factor in observations in the reflection mode, while shot noise dominates in the fluorescence mode. With recent PMT models (e.g., from Hamamatsu), detector dark noise is extremely low, same as secondary emission noise, and both can be neglected in most practical applications (see Details "Sources of Noise").
Therefore, the explanations below are focused on the influence of shot noise on lateral resolution.

Fig. 15 As shown in Part 1, small pinhole diameters lead to improved resolution (smaller FWHM, deeper dip – see normalized graph on the left).
The graph on the right shows, however, that constricting the pinhole is connected with a drastic reduction in signal level. The drop in intensity is significant from PH <1 AU to PH = 0.05.

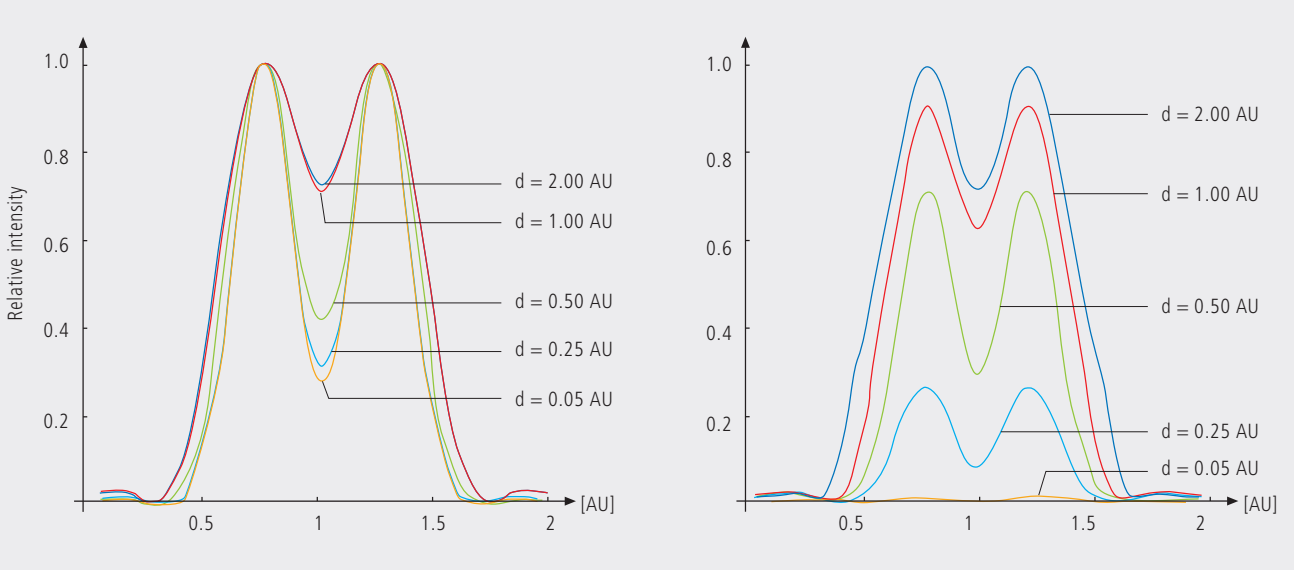

Resolution and shot noise – resolution probability

If the number of photons detected (N) is below 1000, fluorescence emission should be treated as a stochastic rather than a continuous process; it is necessary, via the shot noise, to take the quantum nature of light into account (the light flux is regarded as a photon flux, with a photon having the energy $E = h \cdot \nu$). Resolution becomes contingent on random events (the random incidence of photons on the detector), and the gain in resolution obtainable by pinhole constriction is determined by the given noise level. Figure 16 will help to understand the quantum nature of light.

As a possible consequence of the shot noise of the detected light, it may happen, for example, that noise patterns that change because of photon statistics, degrade normally resolvable object details in such a way that they are not resolved every time in repeated measurements. On the other hand, objects just outside optical resolvability may appear resolved because of noise patterns modulated on them. Resolution of the "correct" object structure is the more probable the less noise is involved, i.e. the more photons contribute to the formation of the image.

Therefore, it makes sense to talk of resolution probability rather than of resolution. Consider a model which combines the purely optical understanding of image formation in the confocal microscope (PSF) with the influences of shot noise of the detected light and the scanning and digitization of the object. The essential criterion is the discernability of object details.

Figure 17 (page 24) shows the dependence of the resolution probability on signal level and pinhole diameter by the example of a two-point object and for different numbers of photoelectrons per point object. [As the image of a point object is covered by a raster of pixels, a normalization based on pixels does not appear sensible.]

Thus, a number of 100 photoelectrons/point object means that the point object emits as many photons within the sampling time as to result in 100 photoelectrons behind the light-sensitive detector target (PMT cathode). The number of photoelectrons obtained from a point object in this case is about twice the number of photoelectrons at the maximum pixel (pixel at the center of the Airy disk). With photoelectrons as a unit, the model is independent of the sensitivity and noise of the detector and of detection techniques (absolute integration time / point sampling / signal averaging). The only quantity looked at is the number of detected photons.

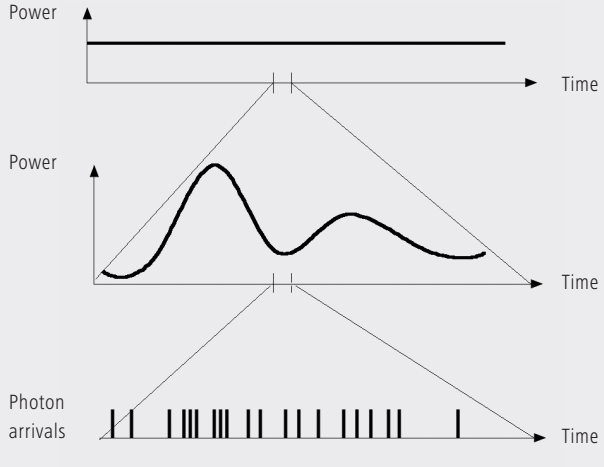

Fig. 16 The quantum nature of light can be made visible in two ways:
- *by reducing the intensity down to the order of single photons and*
- *by shortening the observation time at constant intensity, illustrated in the graph below: The individual photons of the light flux can be resolved in their irregular (statistical) succession.*

A resolution probability of 90% is considered necessary for resolving the two point images. Accordingly, the two-point object defined above can only be resolved if each point produces at least about 25 photoelectrons. With pinhole diameters smaller than 0.25 AU, the drastic increase in shot noise (decreasing intensity of the detected light) will in any case lead to a manifest drop in resolution probability, down to the level of indeterminateness (≤ 50% probability) at PH = 0.

As another consequence of shot noise, the curve maximum shifts toward greater pinhole diameters as the number of photoelectrons drops.

The general slight reduction of resolution probability towards greater pinhole diameters is caused by the decreasing effectiveness of the pinhole (with regard to suppression of out-of-focus object regions, see Part 1).

The pinhole diameter selected in practice will therefore always be a trade-off between two quality parameters: noise (SNR as a function of the intensity of the detected light) and resolution (or depth discrimination). The pinhole always needs a certain minimum aperture to allow a minimum of radiation (depending on the intensity of fluorescence) to pass to the detector.

Where fluorescence intensities are low, it may be sensible to accept less than optimum depth discrimination so as to obtain a higher signal level (higher intensity of detected light = less noise, better SNR). For most fluorescent applications a pinhole diameter of about 1 AU has turned out to be the best compromise.

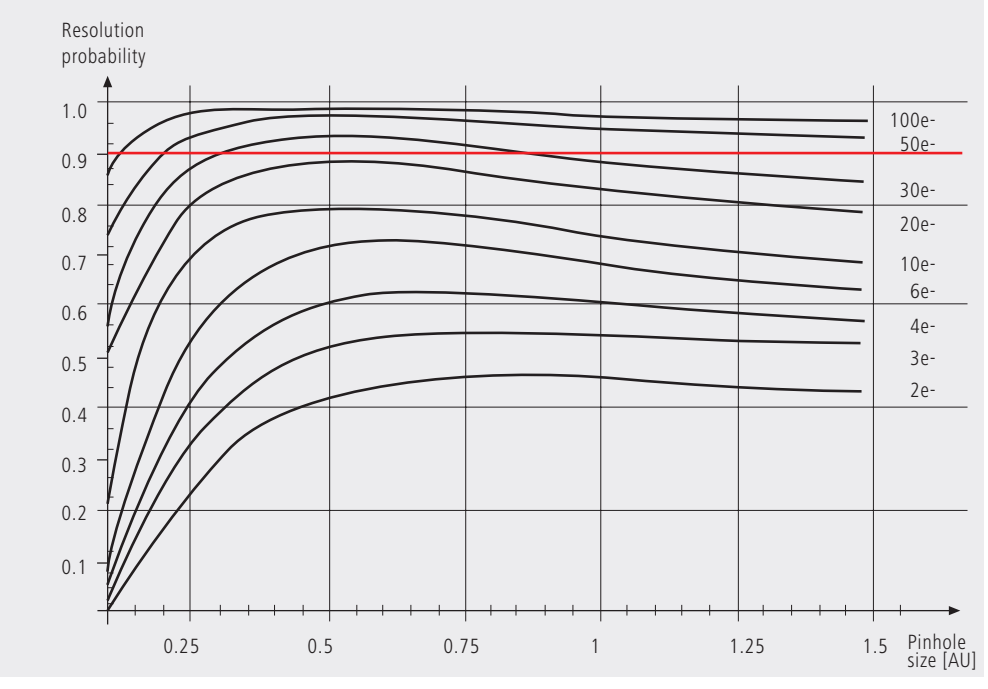

Fig. 17 The graph shows the computed resolution probability of two self-luminous points (fluorescence objects) spaced at 1/2 AU, as a function of pinhole size and for various photoelectron counts per point object (e-). The image raster conforms to the Nyquist theorem (critical raster spacing = 0.25 AU); the rasterized image is subjected to interpolation. The photoelectron count per point object is approximately twice that per pixel (referred to the pixel at the center of the Airy disk). Each curve has been fitted to a fixed number of discrete values, with each value computed from 200 experiments.

The resolution probability is the quotient between successful experiments (resolved) and the total number of experiments. A resolution probability of 70% means that 7 out of 10 experiments lead to resolved structures. A probability > 90% is imperative for lending certainty to the assumption that the features are resolved. If we assume a point-like fluorescence object containing 8 FITC fluorescence molecules (fluorochrome concentration of about 1 nMol) a laser power of 100 µW in the pupil and an objective NA of 1.2 (n = 1.33), the result is about 45 photoelectrons / point object on the detection side.

Possibilities to improve SNR

Pinhole diameters providing a resolution probability below 90% may still yield useful images if one uses a longer pixel time or employs the signal averaging function. In the former case, additional photons are collected at each pixel; in the latter case, each line of the image, or the image as a whole, is scanned repeatedly, with the intensities being accumulated or averaged. The influence of shot noise on image quality decreases as the number of photons detected increases. As fluorescence images in a confocal LSM tend to be shot-noise-limited, the increase in image quality by the methods described is obvious.

Furthermore, detector noise, same as laser noise at high signal levels, is reduced. The figures on the right show the influence of pixel time (figure 18) and the influence of the number of signal acquisitions (figure 19) on SNR in [dB]. The linearity apparent in the semilogarithmic plot applies to shot-noise-limited signals only. (As a rule, signals are shot-noise-limited if the PMT high voltage needed for signal amplification is greater than 500 V).

A doubling of pixel time, same as a doubling of the number of signal acquisitions, improves SNR by a factor of about $\sqrt{2}$ (3 dB). The advantage of the averaging method is the lower laser load on the specimen, as the exposure time per pixel remains constant. Photon statistics are improved by the addition of photons from several scanning runs (SNR = $\sqrt{n \cdot N}$; N = constant, n = number of scans averaged). By comparison, a longer pixel time directly improves the photon statistics by a greater number N of photons detected per pixel (SNR = $\sqrt{N}$, N = variable), but there is a greater probability of photobleaching or saturation effects of the fluorophores (see also details "Fluorescence").

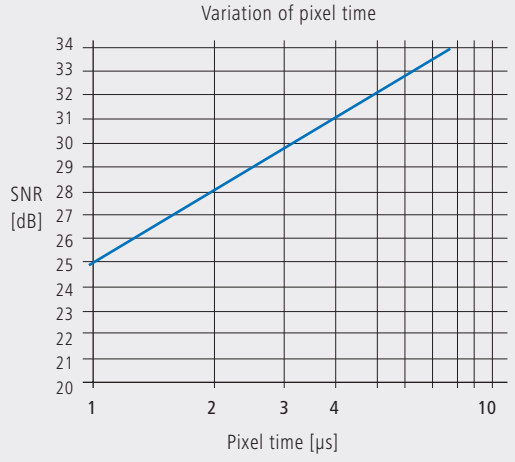

Fig. 18

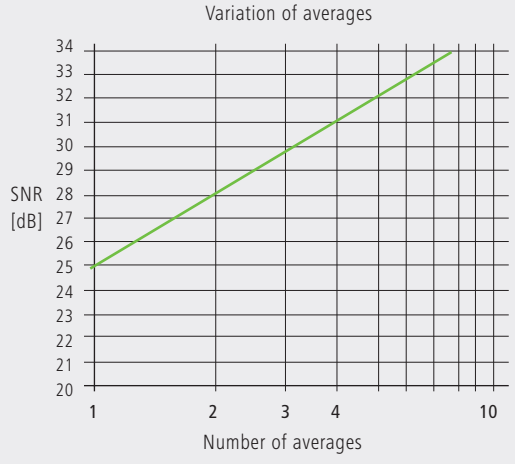

Fig. 19

Figures 18 and 19 Improvement of the signal-to-noise ratio. In figure 18 (top), pixel time is varied, while the number of signal acquisitions (scans averaged) is constant. In figure 19 (bottom), pixel time is constant, while the number of signal acquisitions is varied. The ordinate indicates SNR in [dB], the abscissa the free parameter (pixel time, scans averaged).

a)

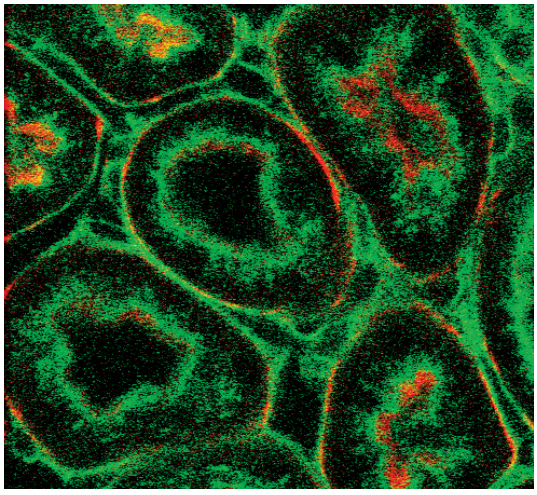

b)

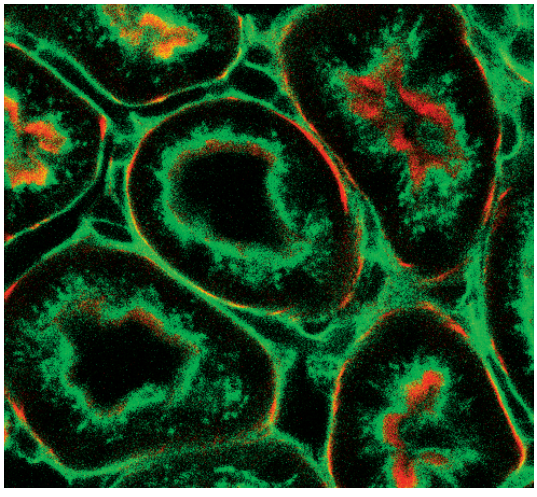

c)

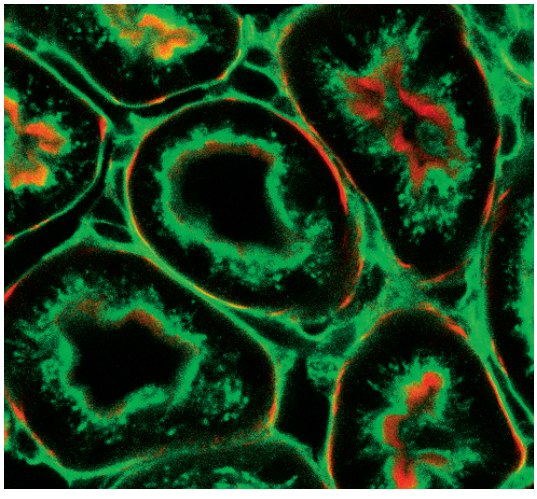

Fig. 20 Three confocal images of the same fluorescence specimen (mouse kidney section, glomeruli labeled with Alexa488 in green and actin labelled with Alexa 564 phalloidin in red).
All images were recorded with the same parameters, except pixel time and average. The respective pixel times were 0.8 µs in a), 6.4 µs (no averaging) in b), and 6.4 µs plus 4 times line-wise averaging in c).

The pictures on the left demonstrate the influence of pixel time and averaging on SNR; object details can be made out much better if the pixel time increases or averaging is employed.

Another sizeable factor influencing the SNR of an image is the efficiency of the detection beam path. This can be directly influenced by the user through the selection of appropriate filters and dichroic beamsplitters. The SNR of a FITC fluorescence image, for example, can be improved by a factor of about 2 (6dB) if the element separating the excitation and emission beam paths is not a neutral 80/20 beamsplitter[1] but a dichroic beamsplitter optimized for the particular fluorescence.

The difficult problem of quantifying the interaction between resolution and noise in a confocal LSM is solved by way of the concept of resolution probability; i.e. the unrestricted validity of the findings described in Part 1 is always dependent on a sufficient number of photons reaching the detector.

Therefore, most applications of confocal fluorescence microscopy tend to demand pinhole diameters greater than 0.25 AU; a diameter of 1 AU is a typical setting.

[1] An 80/20 beamsplitter reflects 20% of the laser light onto the specimen and transmits 80% of the emitted fluorescence to the detector.

Glossary

α	Aperture angle of a microscope objective
AU	Airy unit (diameter of Airy disc)
dpix	Pixel size in the object plane
FWHM	Full width at half maximum of an intensity distribution (e.g. optical slice)
n	Refractive index of an immersion liquid
NA	Numerical aperture of a microscope objective
PH	Pinhole; diaphragm of variable size arranged in the beam path to achieve optical sections
PMT	Photomultiplier tube (detector used in LSM)
PSF	Point spread function
RU	Rayleigh unit
SNR	Signal-to-noise ratio

To give some further insight into Laser Scanning Microscopy, the following pages treat several aspects of particular importance for practical work with a Laser Scanning Microscope.

Pupil Illumination

Optical Coordinates

Fluorescence

Sources of Noise

Pupil Illumination

All descriptions in this monograph suggest a confocal LSM with a ray geometry providing homogeneous illumination at all lens cross sections. It is known that the intensity distribution generated in the focus of the objective lens, is the Fourier transform of the intensity distribution in the objectives pupil plane (backfocal plane). Hence it follows, that a homogeneous distribution in the pupil plane results in a focal distribution following the Airy function (also known as Airy disk) [In Carl Zeiss microscope objectives, the pupil diameter is implemented by a physical aperture close to the mounting surface of the lens].

The Airy distribution is characterized by a smaller width at half maximum and thus by a higher resolving power than a Gaussian distribution. Figur A left shows the normalized intensity distribution at the focal plane as a function of different truncation factor's T (T is the ratio of the laser beam diameter ($1/e^2$) and the pupil diameter of the objective lens). The red curve results at a homogeneous pupil illumination with $T > 5.2$, while the blue one is obtained at a Gaussian pupil illumination with $T \leq 0.5$; the green curve corresponds to a truncation factor T=1.3. The lateral coordinate is normalized in Airy units (AU). From T=3, the Airy character is predominating to a degree that a further increase in the truncation factor no longer produces a gain in resolution. Because of the symmetry of the point image in case of diffraction-limited imaging, the graph only shows the intensity curve in the +X direction. Furthermore any truncation of the illuminating beam cross-section at the pupil plane causes a certain energy loss and thus a decrease in efficiency. Figure A (right) shows the percentage efficiency as a function of pupil diameter in millimeter, with constant laser beam expansion. The smaller the pupil diameter, the higher the T-factor, and the higher the energy loss (i.e. the smaller the efficiency). Example: If the objective lens utilizes 50% of the illuminating energy supplied, this means about 8% resolution loss compared to the ideal Airy distribution. Reducing the resolution loss to 5% is penalized by a loss of 70% of the illuminating energy. In practice, the aim is to reach an optimal approximation to a homogeneous pupil illumination with a reasonable loss in efficiency.

Fig. A

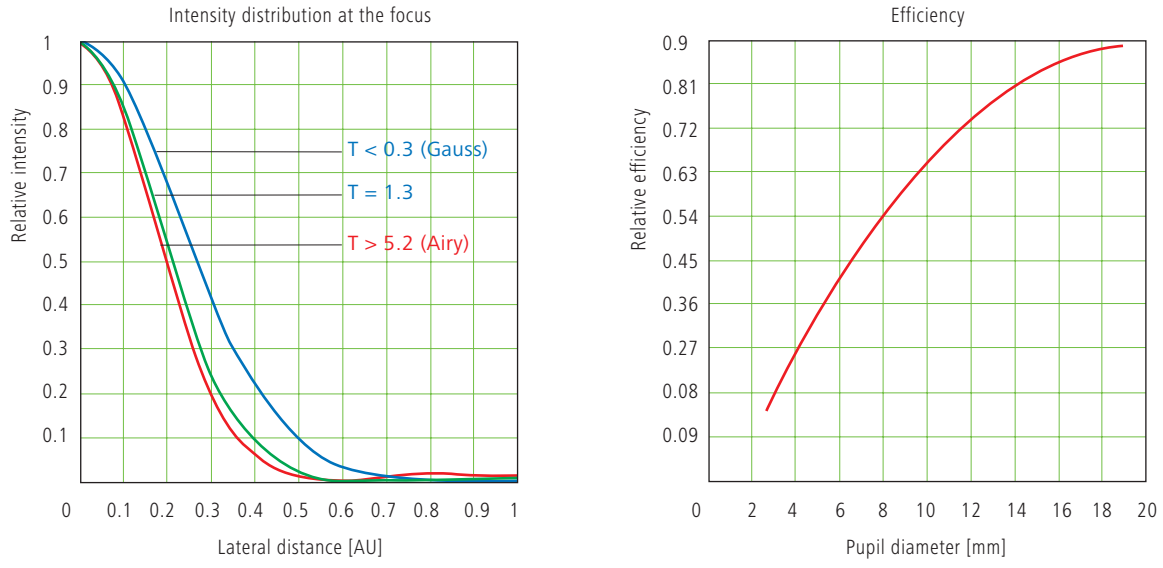

The trunction factor T is defined as the ratio of laser beam diameter ($1/2^2$) and pupil diameter of the objective lens used:

$$T = \frac{d_{laser}}{d_{pupille}}$$ the resulting efficiency is defined as $$\eta = 1 - e^{\left(\frac{-2}{T^2}\right)}$$

The full width at half maximum of the intensity distribution at the focal plane is definied as:

$$FWHM = 0.71 \cdot \frac{\lambda}{NA} \cdot \omega$$ with $$\omega = \sqrt{0.51 + 0.14 \cdot ln\left(\frac{1}{1-n}\right)}$$

With T< 0.6, the Gaussian character, and with T>1 the Airy character predominates the resulting intensity distribution.

Optical Coordinates

In order to enable a representation of lateral and axial quantities independent of the objective lens used, let us introduce optical coordinates oriented to microscopic imaging.

Given the imaging conditions in a confocal microscope, it suggests itself to express all lateral sizes as multiples of the Airy disk diameter. Accordingly, the Airy unit (AU) is defined as:

$$1AU = \frac{1.22 \cdot \bar{\lambda}}{NA}$$

NA = numerical aperture of the objective
$\bar{\lambda}$ *= mean wavelength*
with NA = 1.3 and $\bar{\lambda}$ *= 496 nm → 1AU = 0.465 µm*

The AU is primarily used for normalizing the pinhole diameter.

Thus, when converting a given pinhole diameter into AUs, we need to consider the system's total magnification; which means that the Airy disk is projected onto the plane of the pinhole (or vice versa).

Analogously, a sensible way of normalization in the axial direction is in terms of multiples of the wave-optical depth of field. Proceeding from the Rayleigh criterion, the following expression is known as Rayleigh unit (RU):

$$1RU = \frac{n \cdot \bar{\lambda}}{NA^2}$$

n = refractive index of immersion liquid
with NA = 1.3, $\bar{\lambda}$ *= 496 nm and n = 1.52 → 1RU = 0.446 µm*

The RU is used primarily for a generally valid representation of the optical slice thickness in a confocal LSM.

Fluorescence

Fluorescence is one of the most important contrasting methods in biological confocal microscopy.
Cellular structures can be specifically labeled with dyes (fluorescent dyes = fluorochromes or fluorophores) in various ways. Let the mechanisms involved in confocal fluorescence microscopy be explained by taking fluorescein as an example of a fluorochrome. Fluorescein has its absorption maximum at 490 nm. It is common to equip a confocal LSM with an argon laser with an output of 15–20 mW at the 488 nm line. Let the system be adjusted to provide a laser power of 500 µW in the pupil of the microscope objective. Let us assume that the microscope objective has the ideal transmittance of 100%.
With a C-Apochromat 63x/1.2W, the power density at the focus, referred to the diameter of the Airy disk, then is $2.58 \cdot 10^5$ W/cm^2. This corresponds to an excitation photon flux of $6.34 \cdot 10^{23}$ photons/cm^2 sec. In conventional fluorescence microscopy, with the same objective, comparable lighting power (xenon lamp with 2 mW at 488 nm) and a visual field diameter of 20 mm, the excitation photon flux is only $2.48 \cdot 10^{18}$ photons/cm^2 sec, i.e. lower by about five powers of ten.
This is understandable by the fact that the laser beam in a confocal LSM is focused into the specimen, whereas the specimen in a conventional microscope is illuminated by parallel light.
The point of main interest, however, is the fluorescence (F) emitted.

The emission from a single molecule (F) depends on the molecular cross-section (σ), the fluorescence quantum yield (Qe) and the excitation photon flux (I) as follows:

$$F = \sigma \cdot Qe \cdot I \quad \text{[photons/sec]}$$

In principle, the number of photons emitted increases with the intensity of excitation. However, the limiting parameter is the maximum emission rate of the fluorochrome molecule, i.e. the number of photons emittable per unit of time. The maximum emission rate is determined by the lifetime (= radiation time) of the excited state. For fluorescein this is about 4.4 nsec (subject to variation according to the ambient conditions). On average, the maximum emission rate of fluorescein is $2.27 \cdot 10^8$ photons/sec. This corresponds to an excitation photon flux of $1.26 \cdot 10^{24}$ photons/cm^2 sec. At rates greater than $1.26 \cdot 10^{24}$ photons/cm^2 sec, the fluorescein molecule becomes saturated. An increase in the excitation photon flux will then no longer cause an increase in the emission rate; the number of photons absorbed remains constant. In our example, this case occurs if the laser power in the pupil is increased from 500 µW to roughly 1mW. Figure B (top) shows the relationship between the excitation photon flux and the laser power in the pupil of the stated objective for a wavelength of 488 nm. Figure B (bottom) illustrates the excited-state saturation of fluorescein molecules. The number of photons absorbed is approximately proportional to the number of photons emitted (logarithmic scaling).

The table below lists the characteristics of some important fluorochromes:

	Absorpt. max.(nm)	$\sigma/10^{-16}$	Qe	σ*Q/10^{-16}
Rhodamine	554	3.25	0.78	0.91
Fluorescein	490	2.55	0.71	1.81
Texas Red	596	3.3	0.51	1.68
Cy 3.18	550	4.97	0.14	0.69
Cy 5.18	650	7.66	0.18	1.37

Source:
Handbook of Biological Confocal Microscopy, p. 268/Waggoner
In the example chosen,
F = $1.15 \cdot 10^8$ photons/sec or 115 photons/µsec

What has been said so far is valid only as long as the molecule is not affected by photobleaching. In an oxygen-rich environment, fluorescein bleaches with a quantum efficiency of about $2.7 \cdot 10^{-5}$. Therefore, a fluorescence molecule can, on average, be excited n = 26.000 times ($n = Q/Q_b$) before it disintegrates.

With $t = \frac{n}{F_{max}}$, and referred to the maximum emission rate, this corresponds to a lifetime of the fluorescein molecule of about 115 µs.

It becomes obvious that an increase in excitation power can bring about only a very limited gain in the emission rate. While the power provided by the laser is useful for FRAP (fluorescence recovery after photobleaching) experiments, it is definitely too high for normal fluorescence applications. Therefore it is highly important that the excitation power can be controlled to fine increments in the low-intensity range.

A rise in the emission rate through an increased fluorophore concentration is not sensible either, except within certain limits. As soon as a certain molecule packing density is exceeded, other effects (e.g. quenching) drastically reduce the quantum yield despite higher dye concentration.

Another problem to be considered is the system's detection sensitivity. As the fluorescence radiated by the molecule goes to every spatial direction with the same probability, about 80% of the photons will not be captured by the objective aperture (NA = 1.2).

With the reflectance and transmittance properties of the subsequent optical elements and the quantum efficiency of the PMT taken into account, less than 10% of the photons emitted are detected and converted into photoelectrons (photoelectron = detected photon).

In case of fluorescein (NA=1.2, 100 µW excitation power, λ = 488 nm), a photon flux of F~23 photons/µsec results. In combination with a sampling time of 4 µsec/pixel this means 3–4 photoelectrons/molecule and pixel.

In practice, however, the object observed will be a labeled cell. As a rule, the cell volume is distinctly greater than the volume of the sampling point. What is really interesting, therefore, is the number of dye molecules contained in the sampling volume at a particular dye concentration. In the following considerations, diffusion processes of fluorophore molecules are neglected. The computed numbers of photoelectrons are based on the parameters listed above.

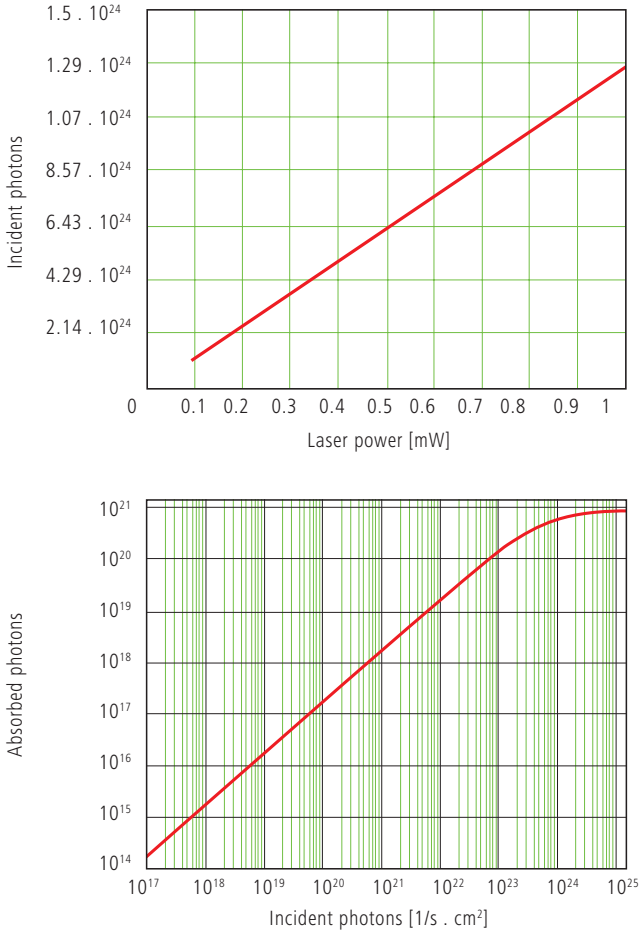

Fig. B Excitation photon flux at different laser powers (top) and excited-state saturation behavior (absorbed photons) of fluorescein molecules (bottom).

With λ = 488 nm and NA = 1.2 the sampling volume can be calculated to be $V = 12.7 \cdot 10^{-18}$ l. Assuming a dye concentration of 0.01 µMol/l, the sampling volume contains about 80 dye molecules. This corresponds to a number of about 260 photoelectrons/pixel. With the concentration reduced to 1 nMol/l, the number of dye molecules drops to 8 and the number of photoelectrons to 26/pixel.

Finally it can be said that the number of photons to be expected in many applications of confocal fluorescence microscopy is rather small (<1000). If measures are taken to increase the number of photons, dye-specific properties such as photobleaching have to be taken into account.

Sources of Noise

Sources of noise effective in the LSM exist everywhere in the signal chain – from the laser unit right up to A/D conversion. Essentially, four sources of noise can be distinguished:

Laser noise q

Laser noise is caused by random fluctuations in the filling of excited states in the laser medium. Laser noise is proportional to the signal amplitude N and therefore significant where a great number of photons (N<10000) are detected.

Shot noise (Poisson noise)

Shot noise is caused by the quantum nature of light. Photons with the energy $h \cdot \upsilon$ hit the sensor at randomly distributed time intervals. The effective random distribution is known as Poisson distribution. Hence,

$$SNR = \Delta N_{Poisson} = \sqrt{N}$$

where N = number of photons detected per pixel time (= photoelectrons = electrons released from the PMT cathode by incident photons). With low photoelectron numbers (N <1000), the number N of photons incident on the sensor can only be determined with a certainty of $\pm\sqrt{N}$.

N can be computed as

$$N = \frac{photons}{QE_{(\lambda)} \cdot pixel\ time}$$

where QE (λ) = quantum yield of the sensor at wavelength λ; 1 photon = h·c/λ; c = light velocity; h = Planck's constant

Secondary emission noise

Secondary emission noise is caused by the random variation of photoelectron multiplication at the dynodes of a PMT. The amplitude of secondary emission noise is a factor between 1.1 and 1.25, depending on the dynode system and the high voltage applied (gain).

Generally, the higher the PMT voltage, the lower the secondary emission noise; a higher voltage across the dynodes improves the collecting efficiency and reduces the statistical behavior of multiplication.

Dark noise

Dark noise is due to the generation of thermal dark electrons N_d, irrespective of whether the sensor is irradiated. Nd statistically fluctuates about $\sqrt{N_d}$. Dark noise is specified for a PMT voltage of 1000 V; with lower voltages it progressively loses significance.

Dark noise can be reduced by cooling the sensor. However, the reduction is significant only if $N \leq N_d$, e.g. in object-free areas of a fluorescence specimen. In addition, the dark noise must be the dominating noise source in order that cooling of the detector effects a signal improvement; in most applications, this will not be the case.

Additional sources of noise to be considered are amplifier noise in sensor diodes and readout noise in CCD sensors. In the present context, these are left out of consideration. The mean square deviation ΔN from the average ($N+N_d$) of the photoelectrons and dark electrons registered, is

$$\Delta N = se \cdot \sqrt{(N+N_d)\,(1+q^2)}$$

so that the total signal-to-noise ratio can be given as

$$SNR = \sqrt{\frac{N^2}{se^2\,(N+N_d)\,(1+q^2)}}$$

where
N = number of photoelectrons per pixel time (sampling time)
se = multiplication noise factor of secondary emission
q = peak-to-peak noise factor of the laser
N_d = number of dark electrons in the pixel or sampling time

Example:

For N =1000, N_d =100, se =1.2, and q = 0.05

$$SNR = \sqrt{\frac{1000^2}{1.2^2\,(1000+100)\,(1+0.05^2)}} = 25.1$$

Literature

1. Beyer, H.,
Handbuch der Mikroskopie, 2nd Edition, VEB Verlag Technik Berlin, (1985)

2. Born & Wolf,
Priniples of Optics, 6th edition 1988, Pergamon Press

3. Brismar, H., Trepte, O., Ulfhake, B.:
Spectra and Fluorescence Lifetimes of Lissamine, Rhodamine etc....: Influences of Some Environmental Factors Recorded with a Confocal Laser Scanning Microscope, The Journal of Histochemistry and Cytochemistry, Vol. ***43****, pp. 699-707, (7/1995)*

4. Cox, G.,
Optical Imaging Techniques in Cell Biology, CRC Press (2007)

5. Keller, H.E.,
Objective Lens for Confocal Microscopy, Handbook of Biological Confocal Microscopy, pp. 111-125, Plenum Press, 2nd Edition (1995)

6. Gröbler, B.,
Untersuchungen zur Bildübertragung in abtastenden Mikroskopen unter besonderer Berücksichtigung der 3D-Abbildung, PhD thesis, University of Potsdam, (1995)

7. Hell, S., et al.,
Aberrations in confocal fluorescence microscopy induced by mismatches in refractive index, Journal of Microscopy, Vol. ***169****, pp. 391-405 (3/1993)*

8. Hibbs, A. H.,
Confocal Microscopy for Biologists, Kluwer Academic / Plenum Publishers (2004)

9. Nitschke, R.,Wilhelm, S., et al.,
A modified confocal laser scanning microscope allows fast ultraviolet ratio imaging of intracellular Ca2+ activity using Fura 2, Euro. J. Physiologie, Vol. ***433****: pp. 653-663, (1997)*

10. Oldenbourg, R. et al.,
Image sharpness and contrast transfer in coherent confocal microscopy, Journal of Microscopy Vol. ***172****, pp. 31-39, (10/1993)*

11. Pawley, J.,
Handbook of Biological Confocal Microscopy, Springer, 3rd Edition (2006)

12. Stelzer, E.H.K.,
The intermediate optical system of laser scanning confocal microscopes; Handbook of Biological Confocal Microscopy, pp. 207-220. Springer, 3rd Edition (2006)

13. Stelzer, E.H.K., et. al.,
Nondestructive sectioning of fixed and living specimens using a confocal scanning laser fluorescence microscope: Microtomoscopy; SPIE, Vol. ***809****, pp. 130-136, (1987)*

14. Tanke, H.J., van Oostveldt, P., et al.,
A parameter for the distribution of fluorophores in cells derived from measurements of inner filter effect and reabsorption phenomenon, Cytometry Vol. ***2****, pp. 359-369 (6/1982)*

15. Tsien, R.Y., Waggoner, A.,
Fluorophores for Confocal Microscopy, Handbook of Biological Confocal Microscopy, pp. 338-352. Springer, 3rd Edition (2006)

16. Webb, R.H., Dorey, C.K.,
The Pixelated Image, Handbook of Biological Confocal Microscopy, pp. 55-66, Plenum Press, 2nd Edition (1995)

17. Wilson, T., Carlini, A.R.,
Three dimensional imaging in confocal imaging systems with finite sized detectors; Journal of Microscopy, Vol. ***149****, pp. 51-66, (1/1988)*

18. Wilson, T., Carlini, A.R.,
Size of detector in confocal imaging systems; Optical Letters Vol. ***12****, pp. 227-229, (4/1987)*

19. Wilson, T., Sheppard, C.J.R.,
Theory and Practice of Scanning Optical Microscopy, Academic Press, 2nd Edition (1985)

20. Yuste, R., Konnerth, a.,
Imaging in Neuroscience and Development, CSHL Press (2005)

We gratefully acknowledge the assistance of Bernhard Gröbler, Hartmut Heinz and all other staff members who contributed to this brochure.

Carl Zeiss Microscopy GmbH
07745 Jena, Germany
BioSciences
microscopy@zeiss.com
www.zeiss.de/lsm

Information subject to change.
Printed on environmentally friendly paper bleached without chlorine.
60-1-0030/e – printed 11.10
ISBN: 978-3-940885-02-9

Highlights of Laser Scanning Microscopy

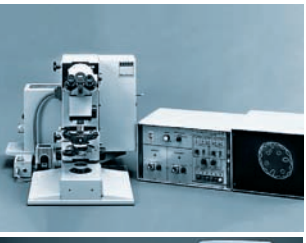

1982
The first Laser Scanning Microscope from Carl Zeiss. The prototype of the LSM 44 series is now on display in the Deutsches Museum in Munich.

1988
The LSM 10 – a confocal system with two fluorescence channels.

1991
The LSM 310 combines confocal laser scanning microscopy with state-of-the-art computer technology.

1992
The LSM 410 is the first inverted microscope of the LSM family.

1997
The LSM 510 – the first system of the LSM 5 family and a major breakthrough in confocal imaging and analysis.

1998
The LSM 510 NLO is ready for multi-photon microscopy.

1999
The LSM 5 PASCAL – the personal confocal microscope.

2000
The LSM is combined with the ConfoCor 2 Fluorescence Correlation Spectroscope.

2001
The LSM 510 META – featuring multispectral analysis.

2004
The LSM 5 LIVE for ultrafast acquisition.

2008
The LSM 710 and LSM 700 – the new generation of sensitivity and flexibility.

This monograph comprehensively deals with the quality parameters of resolution, depth discrimination, noise and digitization, as well as their mutual interaction.
The set of equations presented allows in-depth theoretical investigations into the feasibility of carrying out intended experiments with a confocal LSM.

ZEISS

We make it visible.